

Comparisons between EISCAT observations and model calculations of the high latitude ionosphere

S. QUEGAN

Department of Applied and Computational Mathematics, University of Sheffield, Sheffield, U.K.

R. S. GILL

Marconi Research Centre, Chelmsford, U.K.

and

M. LOCKWOOD

Rutherford Appleton Laboratory, Didcot, U.K.

(Received in final form 21 March 1988)

Abstract— Calculations using a numerical model of the convection dominated high latitude ionosphere are compared with observations made by EISCAT as part of the UK-POLAR Special Programme. The data used were for 24–25 October 1984, which was characterized by an unusually steady IMF, with $B_z < 0$ and $B_y > 0$; in the calculations it was assumed that a steady IMF implies steady convection conditions. Using the electric field models of HEPPNER and MAYNARD (1983) appropriate to $B_y > 0$ and precipitation data taken from SPIRO *et al.* (1982), we calculated the velocities and electron densities appropriate to the EISCAT observations. Many of the general features of the velocity data were reproduced by the model. In particular, the phasing of the change from eastward to westward flow in the vicinity of the Harang discontinuity, flows near the dayside throat and a region of slow flow at higher latitudes near dusk were well reproduced. In the afternoon sector modelled velocity values were significantly less than those observed. Electron density calculations showed good agreement with EISCAT observations near the F -peak, but compared poorly with observations near 211 km. In both cases, the greatest disagreement occurred in the early part of the observations, where the convection pattern was poorly known and showed some evidence of long term temporal change. Possible causes for the disagreement between observations and calculations are discussed and shown to raise interesting and, as yet, unresolved questions concerning the interpretation of the data. For the data set used, the late afternoon dip in electron density observed near the F -peak and interpreted as the signature of the mid-latitude trough is well reproduced by the calculations. Calculations indicate that it does not arise from long residence times of plasma on the nightside, but is the signature of a gap between two major ionization sources, viz. photoionization and particle precipitation.

1. INTRODUCTION

The last decade has witnessed not only great extensions in the available data on ionospheric behaviour at higher latitudes, but also the construction of a number of numerical models attempting to describe this behaviour (KNUDSEN *et al.*, 1977; WATKINS, 1978; SOJKA *et al.*, 1981a and b, 1982a, 1984, 1985; QUEGAN *et al.*, 1982).

Such models have been successful in reproducing several of the large scale structures present in the high latitude ionosphere, such as the mid-latitude density trough, and in clarifying the role of such processes as ion heating in modifying the ion composition of the ionosphere. They have undoubtedly contributed significantly to our general understanding of the com-

plicated interactions giving rise to observed features of the ionosphere. However, comparison of model calculations with observations has usually been a highly qualitative exercise. This reflects the fact that models need to be driven by inputs and the information available on these input parameters has not been sufficiently detailed for long enough periods to allow simulations covering the many hours necessary to generate sensible modelling. Nonetheless, efforts have been made to reproduce observations (SOJKA *et al.*, 1982b, 1983) and to more closely relate model predictions to data.

Quantitative comparison of model calculations with particular observations serves three important roles:

(a) It is essential if the models are to be validated.

This is not only of pure scientific importance, but is also essential if models are to become useful tools for engineers designing HF systems for operation at high latitudes.

(b) It contributes significantly towards interpretation of the observations, since account must be taken of the full range of physical processes leading to the observations. The relative importance of different physical phenomena, such as convection-induced enhancement of reaction rates (SCHUNK and RAITT, 1980), or stagnation in a region of low ionization rate (SPIRO *et al.*, 1978) is accurately defined. It is far too easy when explaining observations qualitatively to pick out only one process and to ignore other interacting processes which may counteract, add to or even outweigh the one selected.

(c) It makes clear how ignorance of one or more parameters can introduce large uncertainty into the expected behaviour and hence into our ability to understand the observations.

This paper describes the results of an attempt to reproduce quantitatively some *F*-region observations from EISCAT, when the Interplanetary Magnetic Field, which is a major controlling influence on the high latitude *F*-region, was unusually stable over a prolonged period. These conditions, though rare, provide an ideal opportunity to make qualitative testing of the model. The data, the reasons for its selection and its interesting features are described in Section 2. Section 3 describes the model formulation and the input parameters used to drive the model. In Section 4 we present the major results, which are a comparison of both convection velocities and electron densities observed by EISCAT with model calculations. Section 5 discusses the implication of these results and their relevance to other observations.

2. DATA SELECTION

The underlying aim of this study was to establish whether the simple model described in Section 3 with non-varying input parameters is able to reproduce EISCAT observations on particular days. Only a single day is discussed here. In order to reduce the difficulties in defining inputs, the EISCAT data selected was from the UHF Special Programme UK-POLAR [for a full description see VAN EYKEN *et al.* (1984) and WILLIS *et al.* (1986)]. In this observing mode, EISCAT is almost looking towards the magnetic north pole and is observing as far as possible into the convection dominated ionosphere. This removes the ambiguity possible when using, e.g. data from EISCAT's Common Programme, CPO (looking along the magnetic

meridian at Tromsø), where the observed plasma may be either convection or co-rotation dominated, depending on the UT and magnetic conditions (LOCKWOOD *et al.*, 1984; FARMER *et al.*, 1984). As a result, we expect field aligned outflows from the ionosphere to the magnetosphere at all times, rather than a diurnal ebb and flow of plasma (BANKS and KOCKARTS, 1973).

The other major advantage of UK-POLAR is its high time resolution, producing velocity vectors every 2.5 min by the beamswinging technique and scalar data (densities and temperatures) every 15 s. Here we use scalar data which have been post-integrated into 2 min periods, with one such period from each of two viewing directions in the 5 min beamswinging cycle period. Frequently, when making comparisons with modelled values, we will further average the data over longer periods. However, it is important to realize that the data are collected almost continuously throughout these post integration periods (data taken while the antenna is in motion are not used), not just during small periods of a scan cycle (for example the half-hour cycle of EISCAT's Common Programme CP-3). The high time resolution is achieved by UK-POLAR at the expense of coverage of latitudes near and to the south of Tromsø, but enables us to ensure that neither the convection pattern nor the spatial distribution of plasma density have undergone rapid (to the order of minutes) changes of the kinds recently reported using UK-POLAR data by RISHBETH *et al.* (1985) and LOCKWOOD *et al.* (1986a, b).

Observations on 24–25 October 1984 (see WILLIS *et al.*, 1986) were selected because untypically, they include an extended period of steady IMF and convection conditions, as is shown in Fig. 1. The upper panels in this figure show the components of the IMF as observed on this day by AMPTE-UKS at a location just sunward of the Earth's bow shock. From 0600 UT (when observations became available) B_z is small and negative, B_y is consistently positive and B_x is negative. Steady conditions in the IMF are expected to give rise to a constant reconnection rate at the dayside magnetopause and a constant cross tail potential (REIFF *et al.*, 1981; DOYLE and BURKE, 1983; WYGANT *et al.*, 1983), though possibly modulated by the UT variation of the orientation of the Earth's magnetic field (MENG, 1979). The convection electric field at ionospheric heights is therefore expected to be approximately time independent and the work described in this study makes this assumption. When velocity data observed by UK-POLAR are studied carefully it is found that this is far from the case on a timescale of minutes (TODD *et al.*, 1987) or tens of minutes (ETEMADI *et al.*, 1987, 1988). However, what

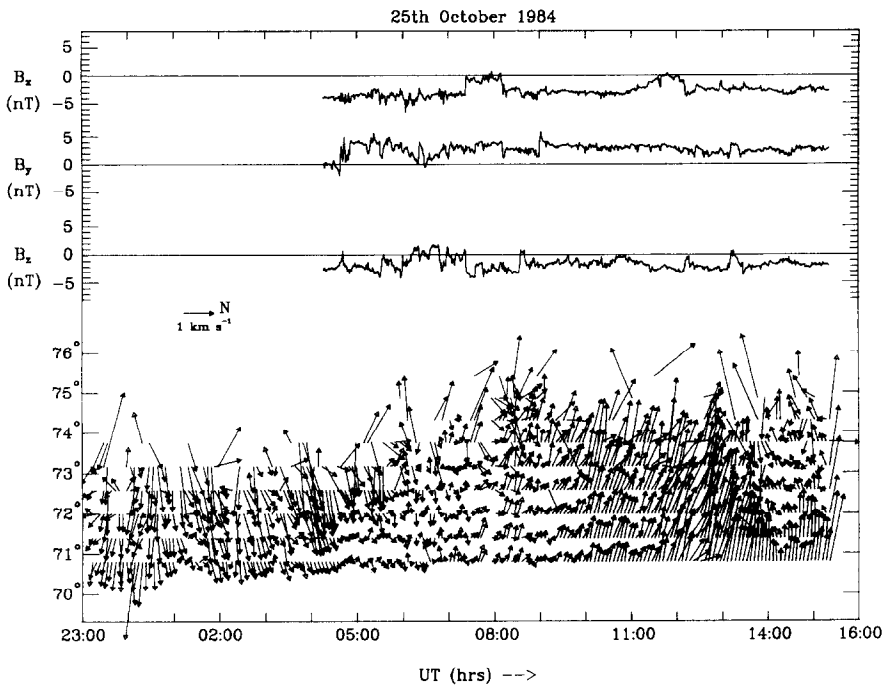


Fig. 1. One minute integration of IMF components (GSM coordinates) observed by AMPTE-UKS and AMPTE-IRM on 24–25 October (top three panels). 2.5 min resolution EISCAT velocity vectors (bottom panel) observed over the same period, shown as a function of UT. In the plot, northward (poleward) velocities point to the right and eastward velocities point downwards.

is important here is that the convection data show no trends over periods of half an hour or greater. The lower panel in Fig. 1 shows plasma convection velocities as a function of UT. Note that, to prevent congestion, the predominantly zonal flows are plotted in an 'electric field' format in which westward flow is represented by upward pointing arrows and northward flow by arrows pointing to the right. There is a clear signature of sunward flow in both the morning and afternoon sectors, with particularly strong westward flow in the afternoons. This is shown even more clearly in Fig. 2, which gives a representation of the full set of EISCAT data for this day. This invariant latitude/magnetic local time (MLT) polar plot shows field perpendicular convection vectors, v (10 min averages of four 2.5 min observations), electron density, N_e , and electron and ion temperatures (T_e and T_i) as a series of polar dials. For each dial, latitude and gate number increase inwards and each dial has its own height scale, since each range gate represents a different altitude as well as a different invariant latitude. Values are shown for eight range gates (gate 1 is the nearest to EISCAT, gate 8 is the farthest away); a gap in any gate indicates that the signal-to-noise ratio

for that observation was too low to allow a reliable measurement to be made.

The outermost band in Fig. 2 is another representation of the velocity data shown in Fig. 1 and several interesting features are apparent in these ten minute averages:

(i) The plasma shows sunward flow in the morning and afternoon sectors, with strong westward flows in the afternoon, as already noted. This is consistent with a two cell convection pattern, which is expected for the negative B_z conditions observed at this time by AMPTE-UKS (HEELIS and REIFF, 1985).

(ii) Between 1000 and 1100 MLT the convection velocity clearly turns polewards from westward flow, suggesting that we are seeing the limit of the dusk cell and that the separation between the two cells is in the pre-noon sector, in agreement with other observations (see HEELIS and REIFF, 1985 for references). The morning side of this velocity rotation is a region of slow flow, showing no real sign of a dawn convection cell. Note that the velocities shown in Figs. 1 and 2 are in a frame which is co-rotating with the radar. Hence the mid-morning plasma is moving sunward with a

velocity only slightly greater than that of co-rotation.

(iii) Velocities on the dawn side show clear eastward flow only in the period 0130–0800 MLT. There is slight evidence for sunward flow (exit from the polar cap) at the earliest times, but in general, observed flows are irregular. At some MLTs flows increase with latitude, at others they decrease and at others there is no obvious organisation with respect to latitude (see also ETEMADI *et al.*, 1988). There is certainly no evidence for the latitudinal dependence discussed by HEPPNER (1977), VOLLAND (1978) and SOJKA *et al.* (1980).

(iv) Plasma is flowing westward throughout the afternoon sector. As the radar rotates to later local times, the latitude of peak westward flow velocity moves from the highest latitudes observed to the lowest latitudes, with a smooth transition. Particularly noticeable in the late afternoon sector are regions of marked westward flow at lower latitudes, and of slow flows at high latitudes. Note again that the co-rotation velocity is not included in the measurement, so this is *not* a stagnation region as that discussed by KNUDSEN (1974) or SPIRO (1978). A similar feature is regularly observed in UK-POLAR data (see surveys by WILLIS *et al.*, 1986; TODD *et al.*, 1987; and ETEMADI *et al.*, 1988).

The above features are consistent with existing knowledge of convection patterns and their relation to the IMF. For $B_z \leq 0$ and $B_y \geq 0$, the convection pattern is expected to be two celled. The dusk cell is approximately circular and occupies much of the polar cap; the dawn cell is crescent shaped and restricted to a small area on the dawn side of the polar cap. The entry region into the polar cap for plasma in the dusk cell extends well into the morning side.

These features are clear in the studies by HEPPNER (1977), HEELIS *et al.* (1983) and HEPPNER and MAYNARD (1987); the latter two studies also indicate that the separation of the two cells is not sun aligned but is rotated into a pre-noon/late evening direction. All these studies concur in finding that flows in the dusk side polar cap are comparatively slow for $B_y > 0$.

The electron concentrations observed by EISCAT are shown in the outermost colour dial of Fig. 2. The most notable features are the regions of enhanced concentrations near magnetic noon and dusk. The morning sector exhibits low densities and little structure (at least for the colour contour levels employed here), while the two regions of enhanced densities are separated by a clear region of low concentration in the afternoon sector; this is a common feature of the EISCAT UK-POLAR data and is normally qualitatively interpreted as the afternoon sector signature

of the mid-latitude trough (WILLIS *et al.*, 1986). As the results of Section 4 will show, the contour levels employed in Fig. 2 hide a number of aeronomically interesting features, particularly as regards the apparently uninteresting morning sector and our interpretation of the afternoon trough.

3. MODEL FORMATION

The calculations described in Section 4 are carried out using a numerical scheme whose basic structure is described by QUEGAN *et al.* (1982), but with the significant improvements described below. The computation proceeds by solving the coupled continuity and momentum equations for a mixture of O^+ and H^+ (referred to by suffixes 1 and 2, respectively) ions in a frame moving with the plasma under the $\mathbf{E} \times \mathbf{B}$ drift. Under these conditions the continuity equation for the O^+ ion takes the form:

$$\frac{dN_1}{dt} = P_1 - L_1 - \frac{\partial}{\partial s}(N_1 v_1), \quad (1)$$

where N_1 is O^+ concentration, t is time, P_1 is the production rate of O^+ , L_1 is the loss rate of O^+ , v_1 is the O^+ field aligned velocity and s is the arc length along a magnetic field line measured towards the equator. The derivative d/dt is the moving derivative for a frame moving with $\mathbf{E} \times \mathbf{B}$ drift. This formulation assumes straight field lines and neglects the effect of field line divergence. The momentum equation for the O^+ ion has the form:

$$0 = -g \sin I - \frac{k}{m_1} \left[\frac{\partial}{\partial s}(T_e + T_i) + \frac{T_i}{N_1} \frac{\partial N_1}{\partial s} + \frac{T_e}{N_e} \frac{\partial N_e}{\partial s} + \beta_1 \frac{\partial T_i}{\partial s} \right] - (1 - \Delta) v_{12}(v_1 - v_2) - v_{in}(v_1 - u \cos I), \quad (2)$$

where g is the acceleration due to gravity, I is the magnetic dip angle, k is Boltzmann's constant, m_1 is the mass of O^+ ion, $N_e = N_1 + N_2$ which is the electron concentration, T_e is the electron temperature, T_i is the ion temperature (assumed the same for all ion species), β_1 is the O^+ thermal diffusion coefficient, Δ is the ordinary thermal diffusion correction term $\sim N_1/(0.66N_2 + 1.563N_1)$ (ST.-MAURICE and SCHUNK, 1977), u is the meridional component of the neutral air wind velocity, v_{12} is the collision frequency for momentum transfer between O^+ and H^+ ions and v_{in} is the collision frequency for momentum transfer between O^+ ions and neutral gases.

The values taken for v_{12} and v_{in} are:

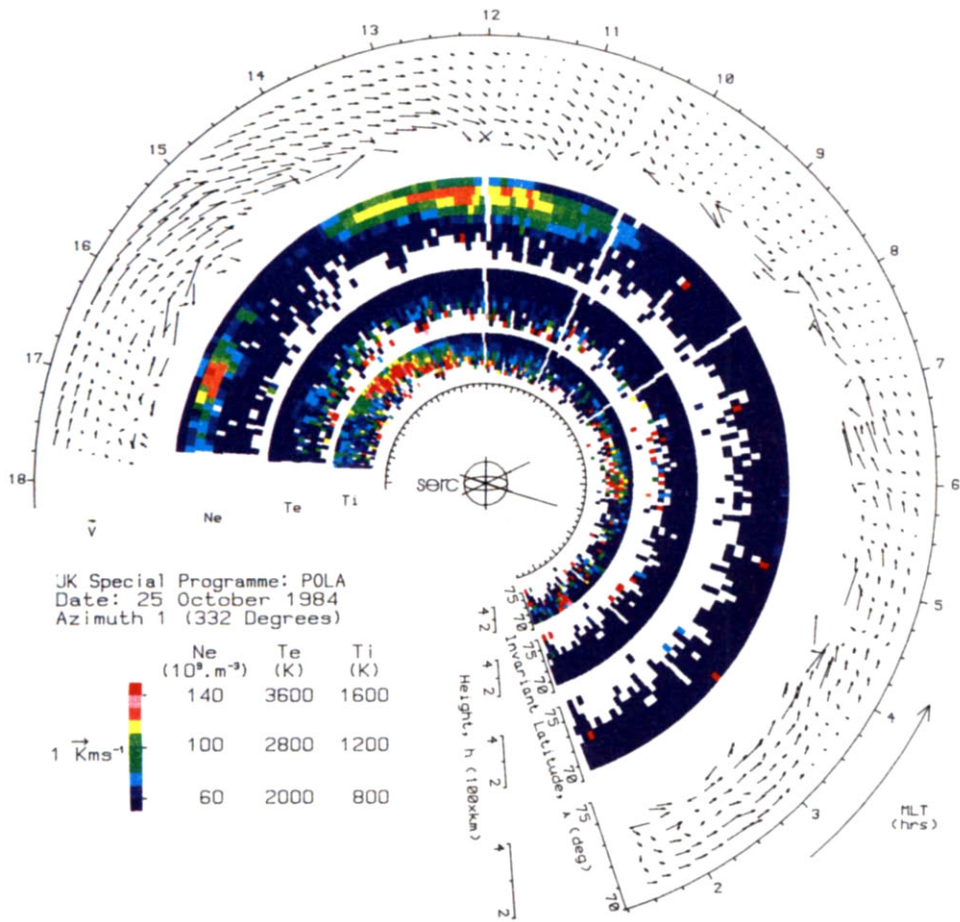


Fig. 2. Polar dial plots of EISCAT data for 25 October 1984, consisting of concentric invariant latitude-MLT plots of 10 min averages of velocity vectors V , plasma density N_e , electron temperature T_e , and ion temperature T_i . Each dial also has a height scale, the height of the observation increasing with range and gate number.

$$v_{12} = 8.4 \times 10^{-8} N_2 / T_i^{1.5} \text{ s}^{-1} \quad (3)$$

and

$$v_{1n} = 3.42 \times 10^{-17} n(\text{O}) T^{0.5} (1.04 - 0.67 \log_{10} T)^2 \\ + 6.66 \times 10^{-16} n(\text{O}_2) + 6.82 \times 10^{-16} n(\text{N}_2) \text{ s}^{-1}, \quad (4)$$

where $T = (T_i + T_n)/2$ and $n(X)$ is the number density of neutral species X .

The calculations for H^+ use equations corresponding to (1) and (2) above. The collision frequencies for H^+ are given by:

$$v_{21} = 1.35 \times 10^{-6} N_1 / T_i^{1.5} \text{ s}^{-1}$$

and

$$v_{2n} = 6.61 \times 10^{-17} n(\text{O}) T_i^{0.5} (1.0 - 0.047 \log_{10} T_i)^2 \\ + 3.20 \times 10^{-15} n(\text{O}_2) + 3.36 \times 10^{-15} n(\text{N}_2) \\ + 2.0 \times 10^{-16} n(\text{H}) T^{0.5} (1.0 - 0.082 \log_{10} T)^2 \text{ s}^{-1}.$$

The values for the above collision frequencies are taken from RAITT *et al.* (1975, 1977).

3.3. Solution of equations

The momentum equation for each ion is rearranged to give an expression for the field aligned flux, which is then substituted in the continuity equation. The resulting diffusion equation is expressed in finite difference form using a fully implicit method, the coefficients being calculated using previously calculated values. At each time step the resulting two systems of linear algebraic equations are solved first for O^+ then for H^+ . At the lower boundary ($z = 120$ km) we take O^+ and H^+ to be in chemical equilibrium, i.e. $P_1 = L_1$ and $P_2 = L_2$. We solve only over the height range 120–1400 km.

The convection paths along which the calculations are carried out are determined by a magnetospheric electric potential model, which is assumed to be time invariant in the magnetic frame. The analytic models of SPIRO (1978) and HEELIS *et al.* (1982) were considered during this study, but all the results presented in Section 4 use a tabulated model for the magnetospheric electric potential due to HEPNER and MAYNARD (1983), as better agreement with the general flow pattern revealed by Fig. 2 could be obtained. The electric field models presented by HEPNER and MAYNARD (1983) have recently been updated (HEPNER and MAYNARD, 1987). The modifications are unlikely to have significant consequences on the calculations presented here, since the major changes necessary were found in the zone from 2130 to 0200 MLT (HEPNER and MAYNARD, 1987), which corresponds to a period which hardly overlaps with the

EISCAT data. As a result, almost no effect would be observed in the modelled velocities and the effects on the calculated electron densities are likely to be small. The total electric potential in a frame fixed with respect to the sun is taken to be the sum of the magnetospheric and the co-rotation potentials. Universal time effects due to the offset between the geomagnetic and geographic axes are properly included using the formulation given by QUEGAN *et al.* (1986). A dipolar form is assumed for the magnetic field, with a dipole situated at geographic coordinates 80°N , 79.6°E (appropriate to the northern hemisphere).

In order to calculate electron densities at points and UTs corresponding to EISCAT observations, a selection of paths was generated. The observed densities represent the integrated effect of a number of processes on plasma which has convected to the observation point. To model these effects, convection paths were tracked backwards in time from a specified geographic location (corresponding to the location of an EISCAT observation gate) and UT. If the convection path entered a region where the solar zenith angle was less than 75° , an initial ion (O^+ and H^+) concentration profile was generated appropriate to steady state conditions under strong photo-ionization. Paths which did not satisfy this condition at any point were tracked back in time for 24 h and an initial steady state profile calculated at this point. This long back-track period removed the sensitivity of the final calculation to the initial plasma profile.

Starting with the assumed initial profile at the appropriate point, the equations (1) and (2) were then solved iteratively along the convection path going forward in time, to yield a single altitude profile of ion concentration at the end point of the path for comparison with the observations.

At each step along the convection path the equation required a number of inputs. The neutral atmospheric concentrations and temperature were taken from the MSIS-83 model (HEDIN, 1983). The neutral wind model was the same as that used in QUEGAN *et al.* (1982); no attempt was made to include a self-consistent wind model, though the ionospheric model described here has been used to perform such calculations (FULLER-ROWELL *et al.*, 1987). The possible effects of this simplification are discussed in Section 4. The expressions for the collision frequencies for momentum transfer, the thermal diffusion coefficients, the flow conditions for O^+ and H^+ at the upper boundary and the procedure for deriving the electron and ion temperatures are all as described in QUEGAN *et al.* (1982). Particle production due to auroral precipitation was calculated using expressions due to REES (1963) and JONES (1974), applied to the

data set prepared by SPIRO *et al.* (1982), based on measurements by the Atmosphere Explorer C and D satellites (this is discussed further in Section 4.2.). Solar photoionization was calculated using photoionization rate coefficients of: 2.0×10^{-7} , 5.1×10^{-7} and $4.5 \times 10^{-7} \text{ s}^{-1}$ for O^+ , O_2^+ and N_2^+ , respectively.

The full electron concentration altitude profile was calculated only at the very last point of the path, for comparison with EISCAT observations. In order to calculate this profile, the coupled ion chemistry of O^+ , NO^+ , O_2^+ , NO , $\text{N}(^2\text{D})$ and $\text{N}(^4\text{S})$ was considered, under the assumption of chemical equilibrium. (In the prior calculations along the convection path, only those reactions involving O^+ or H^+ were considered. This is justified since, by assumption, diffusion effects are only significant in the altitude regime where the molecular ions are minor constituents. As a result, the distributions of O^+ and H^+ will be correctly calculated as long as their chemical links to the molecular ions and neutral constituents are properly catered for as the calculation proceeds along a convection path. Hence, it is only necessary to consider those reactions involving O^+ and H^+ at each step; the final altitude profile would be only slightly affected by including the full calculation for the molecular ions at each step.) A full list of the reactions considered and the associated rate coefficients, is given in the Appendix.

4. COMPARISON OF MODEL CALCULATIONS WITH EISCAT OBSERVATIONS

4.1. Velocity comparisons

Although the principal concern of this study was modelling of electron densities observed by EISCAT, any hope of reproducing observations would require sufficiently accurate modelling of the convection pattern, since this determines the past history of the observed plasma and hence its exposure to production and loss mechanisms. As a result, it was important to investigate the extent to which available models of plasma convection could reproduce the general features of the EISCAT observations noted above. Problems associated with matching observed and model velocities have been discussed by SOJKA and SCHUNK (1986); as they point out, quantitative descriptions of plasma flows embodied in models have only a low order of accuracy, due to the variability in the flows. An average model may not be representative of any one set of observations and precise quantitative agreement between any model and a single set of observations is not to be expected.

Bearing these words in mind, we first attempted to reproduce the observed velocities using an analytic

model based on AE-C data, as formulated by SPIRO (1978) and HEELIS *et al.* (1982). This model not only allows such quantities as the potential difference applied across the polar cap and the cap radius to be supplied as input parameters, but also electric field symmetries, orientation of the convection pattern (relative to the Sun–Earth line) and the width of the dayside entry (throat) and nightside exit regions from the polar cap. However, no way was found to use this flexibility to produce the region of slow flow observed in the dusk section (see Section 2), nor to simulate the flow geometry expected for the observed positive B_y . Accordingly, attempts to use the HEELIS *et al.* (1982) model were abandoned.

Far greater success was achieved for the data shown in Figs. 1 and 2 using a model due to HEPPNER and MAYNARD (1983), which exists in forms appropriate to $B_y \geq 0$ and $B_y \leq 0$. Figure 3 shows the calculated equipotentials of this model for $B_y \geq 0$, based on tabulated data, in a reference frame fixed with respect to the Sun. Note that in this figure the plotted equipotentials are not equally spaced in electric potential. Hence, they indicate the flow geometry, but not the magnitude of the flows. The effects of co-rotation and convection are both apparent in this reference frame. In accordance with the conditions described in Section 2, we used the HEPPNER model for $B_y \geq 0$. However, we translated the whole pattern 4° towards noon and 4° towards dusk in the MLT-invariant latitude frame, in order to match the observed flow geometries near noon (the entry to the polar cap) and late afternoon (the high latitude region of slow flow). These were the only modifications made.

Figure 4 shows the model flow velocities in a form comparable to the outer dial of Fig. 2, i.e. in a co-rotating MLT-invariant latitude reference frame. As noted, translating the original Heppner model reproduces qualitatively the flow behaviour near noon and in the late afternoon. Flow directions are similar in the early afternoon, but modelled flow velocities are too small, particularly around 1500 MLT and at the higher latitudes. In the morning sector the calculated eastward flows are often too large and are much more regular than those observed.

These general observations on the agreement between the observed and model flow characteristics have been placed on a more quantitative footing by examining the magnitude of the zonal flows at range gates 1, 3 and 5, averaged over 12.5 min (see Figs. 5–7, respectively). Stress has been placed on zonal flow, both because it is the dominant flow component (except in the throat region prior to noon) and because of its importance for plasma transport into and out of sunlight. Figure 5 at gate 1 shows general

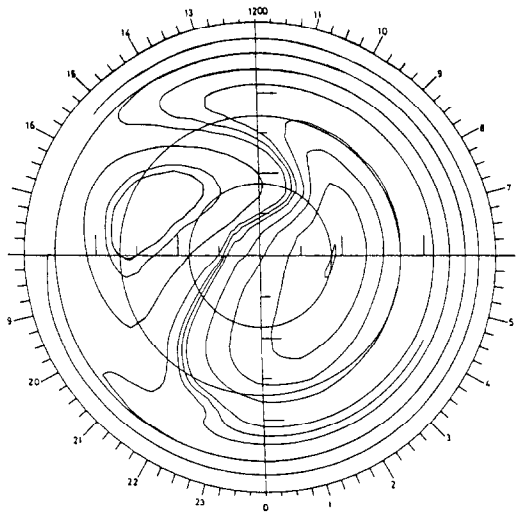


Fig. 3. The polar convection electric potential distribution in the northern hemisphere when the B_y component of the IMF is positive (after HEPPNER and MAYNARD, 1983).

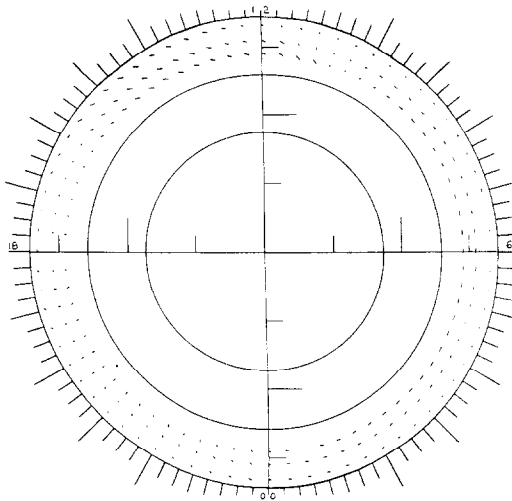


Fig. 4. Model plasma flows in a form comparable to the outer dial of Fig. 2.

agreement between observed and modelled flows, though with some disagreement between the time of change from eastward to westward flow (in the EISCAT data there is no sharp change, rather, there is an extended period of slow flows from about 0700–1200 MLT separating the morning and evening sectors of eastward and westward flow, respectively). Large disagreements are noted near 0200 and from 1500–1800 MLT. The large morning spike may be a sign of higher cross cap potential present when the observations first began, before conditions become more quiescent. The afternoon discrepancy indicates that we have not managed to reproduce the large

westward velocities present in this sector; the model data also decreases too sharply with MLT and does not reproduce well the strong westward flows observed at the lowest latitudes in the late afternoon sector.

Figure 6 compares observed and calculated zonal velocities at gate 3. The phasing of eastward and westward flow is approximately the same for both and flow velocities are in good agreement, except in the afternoon sector, where observed velocities are markedly larger than model velocities. The rapid decrease in velocities in the later afternoon is accurately reproduced.

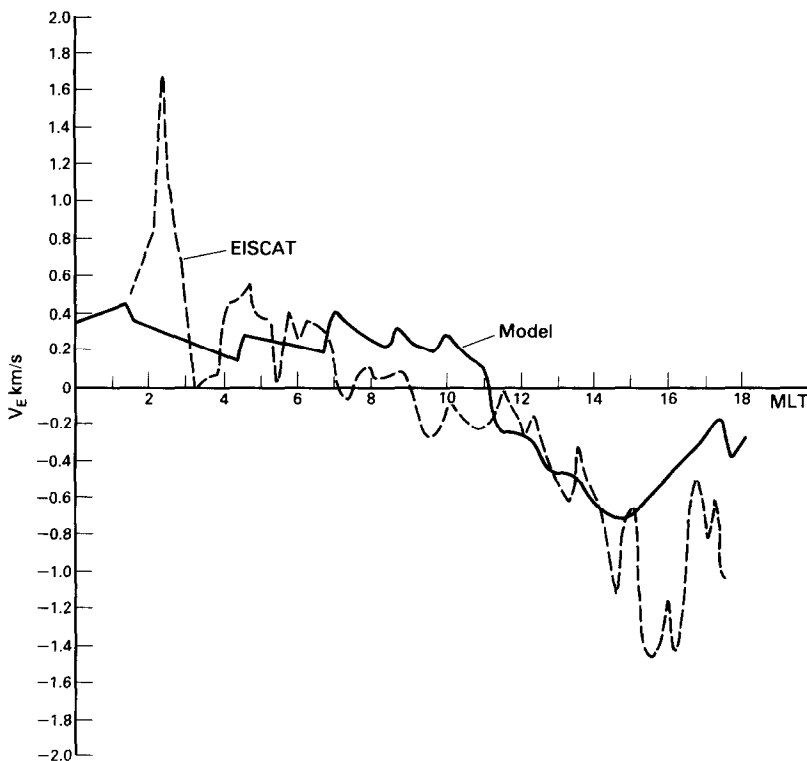


Fig. 5. Observed and calculated eastward velocities corresponding to gate 1 of the observations shown in Fig. 2. The observed velocities shown are $12\frac{1}{2}$ min averages. The calculated velocities are derived from the electric potential distribution shown in Fig. 3, but displaced 4° towards noon and 4° towards dusk in the invariant latitude–MLT frame.

For gate 5 (Fig. 7), the phasing of the direction of the flows is again approximately correct. Very noticeable is the great variability in the observed velocities. In the dawn sector observed velocities oscillate significantly about the model velocities. As for gate 1, there is no sharp change from eastward to westward flow; rather, there is an extended period from ~ 0800 – 1000 MLT separating the two flow regimes. The afternoon sector again shows model velocities significantly smaller than those observed, but the decline in velocities in late afternoon is well represented.

WILLIS *et al.* (1986) and ETEMADI *et al.* (1987b) have considered the experimental errors in the observed zonal flow velocities from the beamswinging technique, due to line-of-sight velocity measurement errors. The latter can be quantified as UK-POLAR makes identical independent observations on five adjacent frequencies and the spread in values is found to rise as the signal-to-background noise level falls (BROMAGE, private communication). Hence, errors in the line-of-sight velocity are dependent on the time of

day (larger plasma densities give larger signal-to-noise ratios), and larger errors are expected for the larger gate numbers (range-squared spatial attenuation and smaller plasma densities for gates above the $F2$ -peak lead to smaller signal levels). For the data set shown in Fig. 2, the line-of-sight velocities have a minimum measurement error near noon, with errors of the order of 5 m s^{-1} at gate 1 growing to 20 m s^{-1} at gate 5. The measurement error is maximal near the start of the observations because of the low plasma densities occurring at these times; the error values are 5 m s^{-1} at gate 1 and 50 m s^{-1} at gate 5 (Bromage, private communication).

The extraction of the zonal and meridional components of velocity from the line-of-sight velocity is also prone to error, whose magnitude depends on the signal-to-noise ratio and on the magnitude of the velocity (stronger flows give greater azimuthal accuracy). A full description of the error analysis is given in WILLIS *et al.* (1986) for the case of stable conditions (which are assumed here); time varying conditions are discussed in ETEMADI *et al.* (1987b). A comprehensive

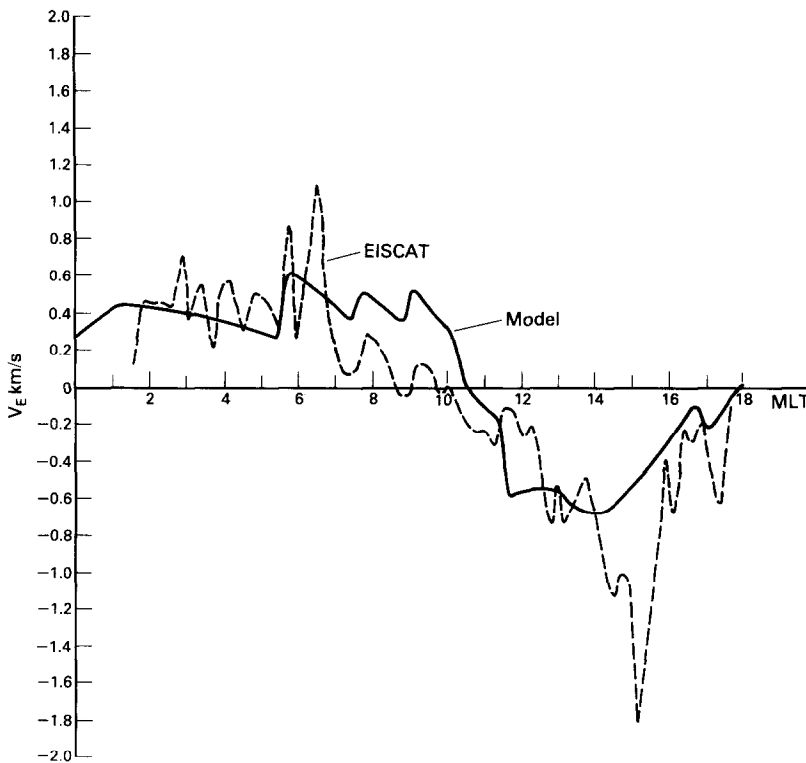


Fig. 6. As Fig. 5, but for gate 3.

azimuthal error analysis for the data shown in Fig. 2 is not straightforward and is not included in the study. However, as representative cases we note that a northward flow of 100 m s^{-1} at noon would have associated errors of 4 m s^{-1} and 4° in azimuth at gate 1, growing to 13 m s^{-1} and 40° at gate 5, while an eastward flow of 1 km s^{-1} in the post-midnight sector would have associated errors of 50 m s^{-1} and 2° in azimuth at gate 1, growing to 180 m s^{-1} and 7° at gate 5. Bearing these values in mind, it is apparent that much of the fluctuation around the model values in Figs. 5–7 is real and not due to observational errors. In Section 4.2 we assess the effects of these fluctuations on the observed plasma densities.

It is interesting to note similarities and dissimilarities in the velocities observed in the three gates because of the bearing this has on the possibility of more accurate convection velocity matching. In the morning sector, there is little correlation in the structure between the three gates, with large spikes appearing only in single gates indicating larger measurement errors due to the lower plasma densities observed. Such behaviour is unlikely to be produced by any model, unless stochastic behaviour is included. In the afternoon sector, similar structure is observed in all

three gates implying real fluctuations in convection. In late afternoon, large velocities persist in gate 1 while gates 3 and 5 show velocities dropping to near zero, a feature thought to be associated with the polar cap boundary being near the further range gates (ETEMADI *et al.*, 1987a). Up to $\sim 1500 \text{ UT}$, velocities in gates 1 and 3 are similar and less than those in gate 5. After this time, the velocities in gate 1 become greater than those in gate 3, which are greater than those in gate 5. The model has not produced the behaviour completely and it is possible that some other choice for the centre of the convection pattern and/or scaling the electric field strength, could produce better agreement with observations for this sector. The values used represent a compromise between the requirements of all local times observed.

To summarise, the Heppner model for $B_y \geq 0$, when shifted 4° towards dusk and noon, appears able to reproduce many of the general features observed in the EISCAT data. The phasing of the change from eastward to westward flow is well reproduced, as are the flows near the throat. In the afternoon sector, model velocity values are significantly lower than those observed. The region of slow flow near dusk is well-reproduced, but the continuing strong westward

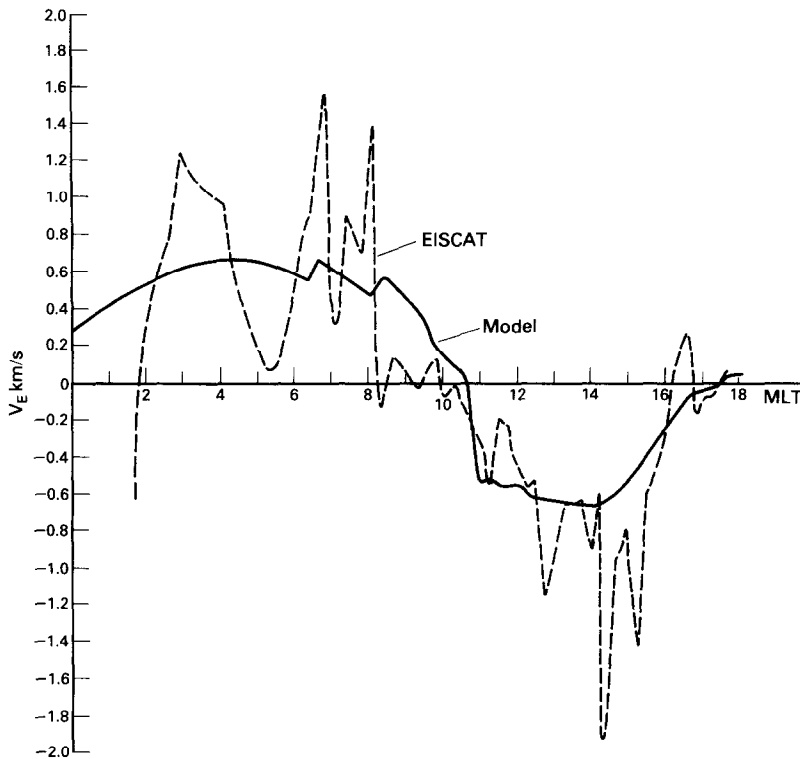


Fig. 7. As Fig. 5, but for gate 5.

flow present in the lowest latitude gate is not present in the model results. The large variability observed in the data is, of course, not present in the model. Differences between the model and the observations have not been properly quantified. Nonetheless, subjectively, the differences between model and data were considered small enough that it was worthwhile proceeding with the calculation of electron densities.

4.2. Electron density comparisons

The means by which electron densities at a given location and UT are calculated has been described in Section 3. In this section we compare the calculated electron densities at gates 1 and 3 with those observed at EISCAT, as illustrated in the dial plot of Fig. 2. The convection pattern used is as described above, and assumed time-invariant.

Correct representation of the precipitation pattern raised difficulties because of the need to make the location of the precipitation consistent with the adopted convection pattern. As discussed in Section 3, the precipitation model used is empirically derived from the AE dataset (SPIRO *et al.*, 1982). The binning used to describe this dataset statistically takes no account of IMF effects [nor of UT effects, which may

be significant; see MAEHLUM (1968) and BURCH (1972)]. As a result, its appropriateness for the steady B_y positive conditions obtained in the observations is unknown. It should also be noted that whereas HEPPNER and MAYNARD (1983) have deliberately avoided smoothing the data in their electric field models, preferring to preserve the sharp boundaries observed in ionospheric convection, the precipitation data of SPIRO *et al.* (1982) is purely statistical, with an associated tendency to smooth out structure, to under-estimate peaks in precipitation and to predict precipitation in regions where, for a specific set of conditions, none or very little may actually occur. In order to take proper account of structure in the precipitation pattern, SOJKA *et al.* (1987) have recently employed DE1 auroral images to give information on the location of the regions of precipitation. However, no such images are available on the day studied here for the northern hemisphere.

As a result, in this study we have been unable to use fully-consistent convection and precipitation data. In order to improve the degree of consistency, we assume that the convection reversal boundary (see Fig. 3) is the region of peak electron precipitation intensity and linearly stretch or compress the latitude

scale along each radius to make the tabulated data of SPIRO *et al.* (1982) meet this condition. This procedure was motivated by the observations of HEELIS *et al.* (1980), who noted that the convection reversal was embedded in the particle precipitation region. However, identifying the convection reversal and peak precipitation region is not necessarily a correct procedure and needs re-evaluation in future work.

The first set of density calculations (Fig. 8) is for gate 3, which observes a volume centred on 277 km, near the *F*-peak. The solid curve shows observed values of electron density and the dashed curves show calculated values; the two dashed curves correspond to SPIRO *et al.* (1982) precipitation data appropriate to $AE \leq 100$ and $100 \leq AE \leq 300$, respectively. Spurious high observed densities due to coherent echoes (e.g. from satellites) have been omitted from the figure. The agreement between observed and calculated values is qualitatively and quantitatively good, although the variability in the data is, of course, not well reproduced. Assuming that this agreement is because the physics have been correctly included in the model, we now interpret the various features of the model results and the data.

In Fig. 3, gate 3 is located at an invariant latitude of 69.5° in the convection pattern, and MLT $\sim UT + 1\frac{1}{2}$ h. Until ~ 1030 UT the plasma is contained on flow lines confined mainly to the dawn side; in the early morning plasma has spent many hours in darkness as it convects across the polar cap and back towards the day side; the possible importance of precipitation is shown in the model data, where reduced precipitation causes significantly lower levels of ionisation. Calculated densities for both AE levels are higher than those observed, although the plasma density shows a dip towards dawn (for low precipitation levels, this dip is to values significantly less than those observed). Towards later times photo-ionisation becomes progressively more important as we move into the day side; the phase and rate of the increase is correctly reproduced by the model.

Particle precipitation becomes of less importance as photo-ionisation becomes the dominant production source. Peak values occur at the same time in the model and data, but the observed day-side peak is wider than the calculated peak. This could be a consequence of the unavailability of particle precipitation data for energies below 300 eV in the AE data set used by SPIRO *et al.* (1982). Measurements by the DMSP series of satellites (HARDY *et al.*, 1985) indicate that in the 12–14 MLT sector such low energy participation can cause considerable additional ionisation. It should also be noted that the calculated noon peak value is a little too high, suggesting an incorrect

neutral atmosphere and/or solar spectrum. The decline from the mid-day peak is correctly produced in the calculations; this decline marks the entry into a circulating plasma cell confined to the dusk side of the polar cap (see Fig. 3). From ~ 1200 UT to the end of the observations the observed plasma is contained within this cell, at first on the outer parts of the cell, then on flow lines near its centre (the polar cap boundary) and then back towards its periphery. In doing so, plasma densities show a marked dip (near ~ 1300 UT) followed by a rise. One of the most pleasing aspects of the model results is the reproduction of this secondary maximum, separated from the noon-time maximum by a significant dip in electron density. It must be remarked that the calculated electron density values in this dip could represent an over-estimate, because of the spreading and smearing of the precipitation values in the SPIRO *et al.* (1982) dataset discussed above.

This dip in electron density is, as noted in Section 2, normally interpreted as the signature of the mid-latitude trough and it is a common feature in the EISCAT data. The dusk-side mid-latitude trough is generally thought of as a consequence of the competition of the co-rotation and magnetospheric electric fields causing plasma to stagnate on the nightside of the terminator, before convecting back towards the dayside (KNUDSEN, 1974; SPIRO, 1978; QUEGAN *et al.*, 1982). This is not the case here. The reduced densities near 1200 UT in the calculations of Fig. 8 occur on convection paths which have not travelled far into the nightside. However, at earlier times there is a peak caused by photoionization, and at later times, we observe increased densities as the observation volume progresses towards the centre of the dusk cell (see Fig. 3) in which there is continual exposure to particle precipitation.

Calculated and observed results for gate 1 (altitude 211 km) are shown in Fig. 9. These results are much less encouraging. The only obvious signs of agreement are the phasing of the rise and fall of the mid-day peak in electron density. The second peak and decline is not well reproduced. Calculated densities at noon are significantly less than those observed, suggesting an incorrect model for the neutral atmosphere. Calculated night-time behaviour is completely different from that observed; observations show a clear maximum near 0300 UT, followed by a rapid decline prior to the dawn increase, as photo-ionisation becomes a dominant influence; calculations show very low values in the morning, significantly affected by precipitation effects and a general increase towards dawn (only at the lowest levels of particle precipitation is there any sign of a dip in the pre-dawn sector).

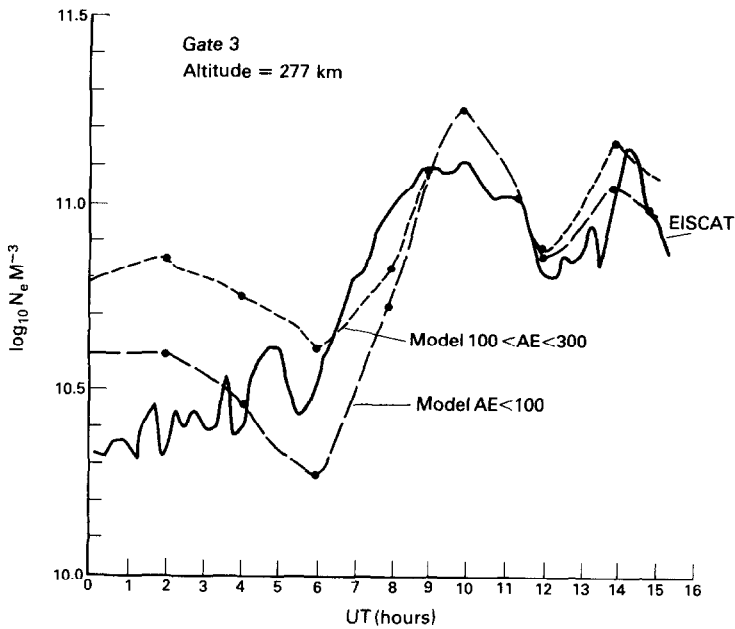


Fig. 8. Observed and calculated electron concentrations corresponding to gate 3 (at an altitude of 277 km) of the observations shown in Fig. 2. The observed concentrations shown are 12½ min averages and spurious values due to coherent echoes have been removed.

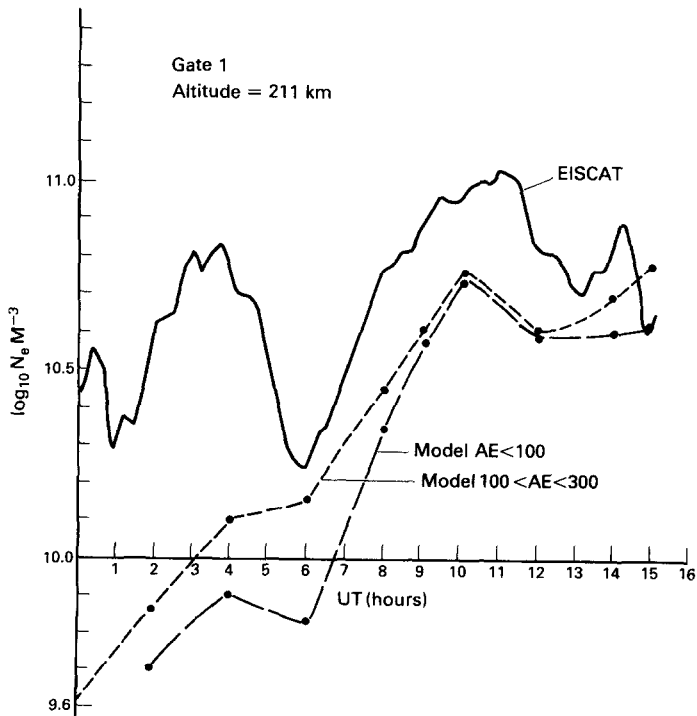


Fig. 9. As for Fig. 8, but for gate 1.

We are therefore faced with three problems—

- (1) What is actually happening to produce the observed morning behaviour?
- (2) Why does the model not reproduce this behaviour?
- (3) Why is agreement poorer at lower altitudes and latitudes?

Before addressing these questions there are some interesting features to note.

Comparison of Figs. 8 and 9 show that the observed behaviours in gates 1 and 3 are fairly similar after 0600. Densities at 211 km are less than those at 277 km at almost all times (the exception is near 1100 UT; electron density at gate 1 reaches its peak at this time, while at gate 3, plasma density is declining; this phase shift is probably due to the different time constants for decay of ionisation at the different altitudes). Prior to 0600, however, observations show quite different behaviour in the two gates. At gate 3, observed densities are fairly flat, although structured. At gate 1 there is a pronounced peak near 0300 UT, followed by a rapid decline. Values at 211 km are significantly higher than those at 277 km during almost all this pre-dawn sector, except in the pre-dawn dip, where values are significantly below. (It should be noted that this aeronomically very interesting state of affairs leaves no signature in the dial plot of Fig. 2, since all plasma densities are in the lowest density colour coding bin. It should further be stressed that the night-time dominance of plasma densities at 211 km compared to 277 km is a long-lasting phenomenon; Figs. 8 and 9 show a genuine progression of observations in time, not a snapshot.)

An attempt to explain the difficulties in reproducing the pre-dawn observations was made by considering a number of processes, including: (i) neutral winds; (ii) plasma convection; (iii) particle precipitation; (iv) local convergence of plasma; (v) ion chemistry.

4.2.1. Neutral winds. In the calculations, the neutral wind model used is the same as that described in QUEGAN *et al.* (1982). No attempt to produce a self-consistent wind pattern was made. On the night-side there are equatorward winds which tend to raise the *F*-layer (in the calculations, the *F*-peak in the morning sectors occurs around 300 km). We performed calculations with the meridional wind set to zero; this had the effect of lowering the *F*-layer to altitudes around 260 km. However, as a result of this lowering, chemical decay increased significantly; calculated densities were of the order of 4.7×10^9 (6.0×10^9) m^{-3} at 211 km and 4.0×10^{10} (1.1×10^{10}) m^{-3} at 277 km with (without) winds included in the calculation, in

altitude profiles calculated at a position corresponding to gate 1 at MLT = 0200. These values are significantly less than those observed. Hence, this calculation seems to show that a reduction in the velocity of the neutral air winds does not help to explain the observations; it does not have the effect of lowering the height of the *F2*-peak and making gate 1 densities greater than those for gate 3, as observed. However, this calculation brings out the importance of neutral winds in this time sector.

4.2.2. Plasma convection. It is not obvious how any appeal to the convection geometry can help, since the observed densities occur in regions of eastward flow at all latitudes. In our flow picture (Fig. 3) the relevant plasma is on one of the outer flow lines of the dawn cell. The plasma at lower latitudes (gate 1) follows a longer convection path than that at higher latitudes (gate 3). Prior to the peak in electron density at 211 km, large eastward flows are observed, mainly at lower latitudes (compare Figs. 5 and 6), which suggests that the assumed convection pattern cannot be correct at the early times. In addition, the long path traversed by this plasma requires a great deal of extrapolation across the polar cap from the convection velocities observed by EISCAT. However, there seems little to be gained by basing any argument on surmises of what that pattern was; nor is it easy to see how to produce the observed differences between gates 1 and 3 for any simple convection pattern, since any two celled pattern would require plasma to spend longer traversing the polar cap and convecting round to the dayside at lower latitudes than at higher. If in this travel the plasma is encountering greater plasma production sources then the observed effects can be brought about. In addition, higher densities could occur if the low latitude plasma was inside the plasmasphere at these times, since this could allow plasma flows from the 'reservoir' of plasma stored in the closed field line region (BANKS and KOCKARTS, 1973). However, this is both unlikely and causes problems in understanding the sharp drop in densities near 0530 UT. It does seem that the possibility of a change in the convection pattern, ending shortly after the start of the observations, and the problems associated with extrapolating the convection equipotentials over the cap could be significant factors in causing all gates to be poorly modelled at the start of the data. If so, this highlights the requirements for accurate convection prediction in modelling high latitude densities.

4.2.3. Particle precipitation. The observations could imply the existence of local production, due to particle precipitation. Schunk (private communication) has noted the sensitivity of the Utah models to particle

precipitation near 200 km. However, this requires the source to be long-lived (several hours), since in order to produce an enhancement, the exposure of plasma to precipitation must have continued for some time, i.e. the plasma must have been convecting through an extended band of precipitation. At the times when the maximum is observed, the convection velocities at gates 1 and 3 are similar (fairly steady at 400 m s^{-1} , i.e. the observed plasma is streaming past EISCAT from the west), hence the precipitation band must be sharply limited to lower latitudes. (The production may be occurring at lower altitudes, but should diffuse to *F*-region heights on a time scale of $\sim 1 \text{ h}$ (SOJKA *et al.*, 1983). Hence a long acting source should leave a signature at gate 3. The lack of such a signature implies the lack of a production source at the gate 3 latitude.) Morning-side precipitation boundaries are not well known and the statistical model of SPIRO *et al.* (1982) is likely to have smoothed out any structure. The averaging involved in this model will also have tended to underestimate true peak precipitation rates and thus peak ionisation rates. Both these features of the data set could have a marked influence on the calculated electron densities. Nonetheless, there seems little justification for suggesting a specific long lived localised production source, such as that discussed above, as a likely cause for the observations.

4.2.4. *Local convergence of plasma.* A possible explanation for the observations resides in the effects of neutral air motions at altitudes near 200 km. FOOTITT *et al.* (1983) have shown that at these altitudes sharp gradients in thermospheric wind velocities can have the effect of concentrating plasma into layers of enhanced density. Their calculations may or may not be valid for the conditions of these observations, but offer some hope for understanding them. The inclusion of such effects in the model would require a refined neutral wind model, including the altitude variation of the meridional wind and the vertical component of the wind. At present we use only the horizontal component of the wind, assumed constant at all altitudes.

4.2.5. *Ion chemistry.* Near 200 km, metallic ions and metastable chemical reactions can be important (Schunk, private communication). These are not included in the model calculations.

Finally, we should more closely analyse what the observations near 211 km actually mean. The densities output by EISCAT form a weighted average of densities over a range gate 75 km long and due to the weighting of autocorrelation function lags contain some information from as low as about 180 km. The region near 200 km is sensitive to a number of processes, as noted above. The apparent value at 211 km

in the EISCAT calculations could reflect enhancements at lower altitudes. By contrast, the model provides a point value at 211 km. (An average value using the EISCAT altitude weighting could be produced, but would have produced little change in the calculated values, since modelled values show no sharp altitude gradients. This reflects the fact that the model contains no inputs which could generate such gradients, even though in the real world, and in particular in the data set under study, such gradients could occur as a result of some of the mechanisms noted above.) Unless the processes giving rise to the enhancements are embodied in the model and the appropriate averaging performed, there is not a proper basis for comparison of the EISCAT and model values. This problem is most acute at the lower altitudes, where narrow layers of ionization can be formed. Near the *F*-region altitude structure is not as pronounced and point and average values are likely to be in greater agreement.

5. SUMMARY

Proper use of the results of model calculations in interpretation of observations and application of models to problems requiring estimates of the spatial distribution of ionospheric densities at high latitudes, are important areas of development. However, such development requires a major effort in validation of model predictions, involving quantitative comparison with observations. The results presented above are a step in this direction. It has been shown that, for untypically steady *By* positive conditions, a convection pattern due to HEPPNER and MAYNARD (1983), when translated 4° towards noon and 4° towards dusk, provided qualitatively good agreement with EISCAT velocity observations. The area of greatest quantitative disagreement was in the afternoon sector, where the magnitudes of modelled westward flows were significantly less than those observed. Elsewhere, quantitative agreement was 'reasonable', though the observed variability in the plasma convection velocities was not produced by the model.

Electron density calculations based on this convection pattern and the SPIRO *et al.* (1982) precipitation pattern (distorted to match the convection reversal with the region of peak precipitation intensity) showed good agreement with EISCAT observations near the *F*-peak at 277 km, but compared poorly with observations near 211 km. In both cases, the greatest area of disagreement was in the early part of the observations, i.e. the post-midnight to dawn sector, where the convection pattern is poorly known

and shows some evidence for long term temporal change. Near the $F2$ -peak, calculated densities were too high. This could be caused by an incorrect particle precipitation model, too rapid transit of plasma from the dayside, or an incorrect value for $hmF2$ due to the neutral wind model used. Near 211 km, calculated densities were too low. Possible explanations for this and for the differences between the observations at 211 and 277 km (changes in convection; localised particle precipitation; plasma localisation by neutral wind gradients; ion chemistry) have not been included in the modelling and would require 'special pleading' in order to be included. This well illustrates the need for extensive knowledge of the input parameters, and in particular the convection pattern, before realistic detailed predictions can be made. The lack of information on conditions prior to the observations makes the interpretation of the morning results impossible.

In terms of understanding, the modelling exercise greatly sharpens any attempt at interpretation of results, since the need to match different processes does not allow arguments leaving out essential elements of the physics. In particular, it calls into question whether the afternoon dip in electron density can be properly regarded as the mid-latitude trough. It also illustrates how important elements of the data can be lost in the presentation, since the morning behaviour which is interesting and hard to understand is invisible in the normal dial plots because of quantization effects.

The more general implications of this work are as yet unknown. We have shown that one set of F -region observations can be reasonably reproduced by making a crude approximation to the convection pattern, combining it with an average precipitation model and an assumed neutral wind pattern and performing a UT dependent calculation. The immediate question is whether other observations can be reproduced.

Work is currently underway to investigate this, including observations under more typical time-dependent conditions.

We can draw some conclusions about the requirements for input parameters. Although an erroneous spatial distribution of particle precipitation is one possible cause of the poorly modelled densities in the post-midnight sector, there are many other possible causes and we note that the relevant part of the convection pattern at these times is poorly known and probably changing. Where we do have good coverage of the relevant part of the convection pattern (i.e. where flows are largely zonal and hence along the band of latitudes covered by the observations) and when the observed flows show no long-term trends, the modelling of densities near the $F2$ -peak is exceptionally good, despite the uncertainties of the precipitation distribution. Hence, it seems a simple fitting of the precipitation model to the convection model, as employed here can be adequate, at least under these 'stable' conditions. It should also be noted that the observed velocities show large fluctuations around the fitted model values, but where these fluctuations are of period ≤ 1 h, the densities are still modelled reasonably well. However, when they are large and of period of several hours or more we do not get good agreement. This is consistent with typical time constants for changes in F -region plasma density.

Acknowledgements—The authors are grateful to D. J. SOUTHWOOD for the provision of AMPTE-UKS magnetometer data, and to B. J. J. BROMAGE and W. C. MIER-JEDRZEJOWICZ for processing the UK-POLAR EISCAT and UKS magnetometer data, respectively. We would also like to give thanks to S. W. H. COWLEY, D. M. WILLIS and R. J. MOFFETT for most helpful discussions of this work and to the Director and staff of EISCAT for their help. EISCAT is supported by the British SERC, French CNRS, West German MPG, Norwegian NAVF, Swedish NFR and Finnish SA. AMPTE is a collaborative project of NASA (USA), MPG (West Germany) and SERC (UK).

REFERENCES

- | | | |
|---|------|--|
| BANKS P. M. and KOCKARTS G. | 1973 | <i>Aeronomy</i> . Academic Press, New York, U.S.A. |
| BURCH J. L. | 1972 | <i>J. geophys. Res.</i> 77 , 6696. |
| DOYLE M. A. and BURKE W. J. | 1983 | <i>J. geophys. Res.</i> 88 , 9125. |
| ETEMADI A., COWLEY S. W. H., LOCKWOOD M.,
BROMAGE B. J. I., WILLIS D. M. and LUHR H. | 1988 | <i>Planet. Space Sci.</i> 36 , 471. |
| ETEMADI A., COWLEY S. W. H. and LOCKWOOD M. | 1987 | <i>J. atmos. terr. phys.</i> , submitted. |
| FARMER A. D., LOCKWOOD M., HORNE R. B.,
BROMAGE B. J. I. and FREEMAN K. S. C. | 1984 | <i>J. atmos. terr. Phys.</i> 46 , 473. |
| FOOTITT R. J., BAILEY G. J. and MOFFETT R. J. | 1983 | <i>Planet. Space Sci.</i> 31 , 671. |
| FULLER-ROWELL T. J., REES D., QUEGAN S.,
MOFFETT R. J. and BAILEY G. J. | 1987 | <i>Pure Appl. Geophys.</i> 127 , 189. |
| HARDY D. A., GUSSENHOVEN M. S. and HOLEMAN E. | 1985 | <i>J. geophys. Res.</i> 90 , 4429. |

- HEDIN A. E. 1983 *J. geophys. Res.* **88**, 10170.
- HEELIS R. A., WINNINGHAM J. D., HANSON W. B. and BURCH J. L. 1980 *J. geophys. Res.* **85**, 3315.
- HEELIS R. A., LOWELL J. K. and SPIRO R. W. 1982 *J. geophys. Res.* **87**, 6339.
- HEELIS R. A., FOSTER J. C., DE LA BEAUJARDIERE O. and HOLT J. 1983 *J. geophys. Res.* **88**, 10111.
- HEELIS R. A. and REIFF P. H. 1985 *Adv. Space Res.* **5**, 349.
- HEPPNER J. P. 1977 *J. geophys. Res.* **82**, 115.
- HEPPNER J. P. and MAYNARD N. C. 1983 *Proc. Chapman Conf.*, Irvington, Virginia, U.S.A.
- HEPPNER J. P. and MAYNARD N. C. 1987 *J. geophys. Res.* **92**, 4467.
- JONES A. V. 1974 *Aurora*, Reidel.
- KNUDSEN W. C. 1974 *J. geophys. Res.* **79**, 1046.
- KNUDSEN W. C., BANKS P. M., WINNINGHAM J. D. and KLUMPAR D. M. 1977 *J. geophys. Res.* **79**, 2868.
- LOCKWOOD M., FARMER A. D., OPGENOORTH H. J. and CROTHERS S. R. 1984 *J. atmos. terr. Phys.* **46**, 489.
- LOCKWOOD M., VAN EYKEN A. P., BROMAGE B. J. I., WILLIS D. M. and COWLEY S. W. H. 1986a *Geophys. Res. Letts.* **13**, 72.
- LOCKWOOD M., VAN EYKEN A. P., BROMAGE B. J. I., WAITE J. H. JR, MOORE T. E. and DOUPNIK J. R. 1986b *Adv. Space Res.* **6**, 93.
- MAEHLUM B. N. 1968 *J. geophys. Res.* **73**, 3459.
- MENG C. I. 1979 *J. geophys. Res.* **84**, 5319.
- OGAWA T. and KONDO Y. 1977 *Planet. Space Sci.* **25**, 735.
- QUEGAN S., BAILEY G. J., MOFFETT R. J., HEELIS R. A., FULLER-ROWELL T. J., REES D. and SPIRO R. W. 1982 *J. atmos. terr. Phys.* **44**, 619.
- QUEGAN S., BAILEY G. J., MOFFETT R. J. and WILKINSON L. C. 1986 *J. atmos. terr. Phys.* **48**, 25.
- RAITT W. J., SCHUNK R. W. and BANKS P. M. 1975 *Planet. Space Sci.* **23**, 1103.
- RAITT W. J., SCHUNK R. W. and BANKS P. M. 1977 *Planet. Space Sci.* **25**, 291.
- REES M. H. 1963 *Planet. Space Sci.* **11**, 1209.
- REIFF P. H., SPIRO R. W. and HILL T. W. 1981 *J. geophys. Res.* **86**, 7639.
- RISHBETH H., SMITH P. R., COWLEY S. W. H., WILLIS D. M., VAN EYKEN A. P., BROMAGE B. J. I. and CROTHERS S. R. 1985 *Nature* **318**, 451.
- ROBLE R. G. and GARRY J. H. 1979 *Geophys. Res. Letts.* **6**, 703.
- ST.-MAURICE J. P. and SCHUNK R. W. 1977 *Planet. Space Sci.* **25**, 907.
- SCHUNK R. W. and RAITT W. J. 1980 *J. geophys. Res.* **85**, 1255.
- SOJKA J. J., FOSTER J. C., RAITT W. J., SCHUNK R. W. and DOUPNIK J. R. 1980 *J. geophys. Res.* **85**, 703.
- SOJKA J. J., RAITT W. J. and SCHUNK R. W. 1981a *J. geophys. Res.* **86**, 609.
- SOJKA J. J., RAITT W. J. and SCHUNK R. W. 1981b *J. geophys. Res.* **86**, 6908.
- SOJKA J. J., SCHUNK R. W. and RAITT W. J. 1982a *J. geophys. Res.* **87**, 187.
- SOJKA J. J., RAITT W. J., SCHUNK R. W., RICH F. J. and SAGALYN R. C. 1982b *J. geophys. Res.* **87**, 1711.
- SOJKA J. J. and SCHUNK R. W. 1984 *J. geophys. Res.* **89**, 2348.
- SOJKA J. J. and SCHUNK R. W. 1985 *J. geophys. Res.* **90**, 5285.
- SOJKA J. J., SCHUNK R. W., EVANS J. V., HOLT J. M. and WAND R. H. 1983 *J. geophys. Res.* **88**, 7783.
- SOJKA J. J. and SCHUNK R. W. 1986 *J. geophys. Res.* **91**, 259.
- SPIRO R. W., HEELIS R. A. and HANSON W. B. 1978 *J. geophys. Res.* **83**, 4255.
- SPIRO R. W., REIFF P. H. and MAHER L. J. JR 1982 *J. geophys. Res.* **87**, 8215.
- ST.-MAURICE J.-P. and TORR D. G. 1978 *J. geophys. Res.* **83**, 969.
- STROBEL D. F., ORAN E. S. and FELDMAN P. D. 1976 *J. geophys. Res.* **81**, 3745.
- TODD H., COWLEY S. W. H., ETEMADI A., BROMAGE B. J. I., LOCKWOOD M., WILLIS D. M. and LUHR H. 1987 *J. atmos. terr. Phys.* **50**, 4230.
- TORR D. G., TORR M. R., BRINTON H. C., BRACE L. H., SPENCER N. W., HEDIN A. E., HANSON W. B., HOFFMAN J. H., NIER A. O., WALKER J. C. G. and RUSCH D. W. 1979 *J. geophys. Res.* **84**, 3360.
- VAN EYKEN A. P., RISHBETH H., WILLIS D. M. and COWLEY S. W. H. 1984 *J. atmos. terr. Phys.* **46**, 635.
- VOLLAND H. 1978 *J. geophys. Res.* **83**, 2695.
- WATKINS B. J. 1978 *Planet. Space Sci.* **26**, 559.

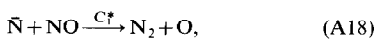
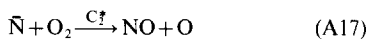
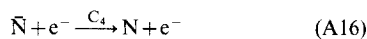
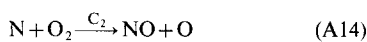
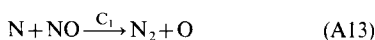
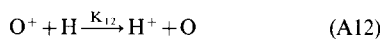
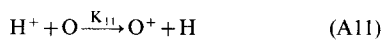
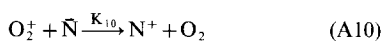
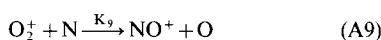
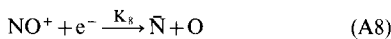
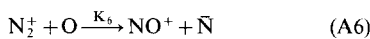
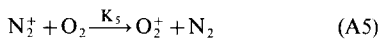
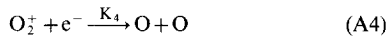
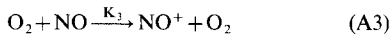
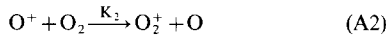
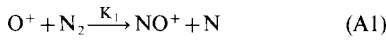
- WILLIS D. M., LOCKWOOD M., COWLEY S. W. H., 1986 *J. atmos. terr. Phys.* **48**, 987.
 VAN EYKEN A. P., BROMAGE B. J. I., RISHBETH H.,
 SMITH P. R. and CROTHERS S. R.
 WYGANT J. R., TORBERT R. B. and MOZER F. S. 1983 *J. geophys. Res.* **88**, 5727.

Reference is also made to the following unpublished material:

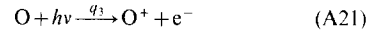
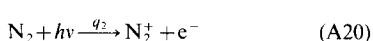
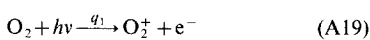
- SPIRO R. W. 1978 Ph.D. thesis, University of Texas at Dallas, Texas, U.S.A.

APPENDIX

The photochemistry of the lower ionosphere is the subject of much recent research and there is no clear universally accepted description of the key reactions, except under particular circumstances (e.g. TORR *et al.*, 1979). As a result, this study used a very extensive chemical scheme (principal sources being ST.-MAURICE and TORR, 1978; RAITT *et al.*, 1975; SCHUNK and RAITT, 1980; OGAWA and KONDO, 1977; STROBEL *et al.*, 1976; ROBLE and GARRY, 1979) involving the following chemical reactions:



where we have written N for N(⁴S) and $\bar{\text{N}}$ for N(²D). Also included are the following photoionisation reactions:



and the photodissociation of NO:



We include in these production rates auroral ionization calculated by the methods described in Section 3. Enhanced dissociation of NO in the auroral zones is not included.

The rate coefficients $K_1 - K_{10}$ and $C_1 - C_4$ have the following values (in $\text{m}^2 \text{s}^{-1}$):

$$K_1 = 1.533 \times 10^{-12} - 5.92 \times 10^{-13} \left(\frac{T_{eff}}{300} \right) + 8.60 \times 10^{-14} \left(\frac{T_{eff}}{300} \right)^2; \quad \text{for } 300 \leq T_{eff} \leq 1700 \text{ K}, \quad (\text{A23})$$

$$K_1 = 2.73 \times 10^{-12} - 1.155 \times 10^{-12} \left(\frac{T_{eff}}{300} \right) + 1.483 \times 10^{-13} \left(\frac{T_{eff}}{300} \right)^2 \quad \text{for } 1700 \leq T_{eff} \leq 6000 \text{ K}, \quad (\text{A24})$$

$$K_2 = 2.82 \times 10^{-11} - 7.74 \times 10^{-12} \left(\frac{T_{eff}}{300} \right) + 1.073 \times 10^{-12} \left(\frac{T_{eff}}{300} \right)^2 - 5.17 \times 10^{-4} \left(\frac{T_{eff}}{300} \right)^3 + 9.65 \times 10^{-16} \left(\frac{T_{eff}}{300} \right)^4 \quad (\text{A25})$$

In equations (A23)–(A25), T_{eff} is an effective temperature defined in ST.-MAURICE and TORR (1978).

$$K_3 = 4.4 \times 10^{-16} \quad (\text{A26})$$

$$K_4 = 1.6 \times 10^{-13} \left(\frac{300}{T_e} \right)^{0.55} \quad (\text{A27})$$

$$K_5 = \frac{1.5 \times 10^{-14}}{T_i} \quad (\text{A28})$$

$$K_6 = 1.4 \times 10^{-16} \left(\frac{300}{T_i} \right)^{0.44} \quad (\text{A29})$$

$$K_7 = 1.8 \times 10^{-13} \left(\frac{300}{T_e} \right)^{0.39} \quad (\text{A30})$$

$$K_8 = 4.2 \times 10^{-13} \left(\frac{300}{T_e} \right)^{0.85} \quad (\text{A31})$$

$$K_9 = 1.8 \times 10^{-16} \quad (\text{A32})$$

$$K_{10} = 2.5 \times 10^{-16} \quad (\text{A33})$$

$$K_{11} = 2.3 \times 10^{-17} T_i^{1/2}$$

(A34) The rate coefficients at the top of the atmosphere are:

$$K_{12} = 2.5 \times 10^{-17} T_n^{1/2}$$

(A35)

$$C_1 = 2.7 \times 10^{-17}$$

(A36)

$$C_1^* = 1.8 \times 10^{-16}$$

(A37)

$$C_2 = 1.1 \times 10^{-20} T_e \exp\left(\frac{-3150}{T_n}\right)$$

(A38)

$$q_1 = 5.1 \times 10^{-7} \text{ s}^{-1} \quad (\text{A42})$$

$$q_2 = 4.5 \times 10^{-7} \text{ s}^{-1} \quad (\text{A43})$$

$$q_3 = 2.0 \times 10^{-7} \text{ s}^{-1} \quad (\text{A44})$$

$$q_4 = 8.6 \times 10^{-6} \text{ s}^{-1}. \quad (\text{A45})$$

$$C_2^* = 7.0 \times 10^{-18}$$

(A39)

$$C_3 = 1.0 \times 10^{-18}$$

(A40)

$$C_4 = 1.35 \times 10^{-16} (T_e - 220)^{1/2}$$

(A41)

for $T_e \geq 220$ K.

In the above expressions, T_e , T_i and T_n are the electron, ion and neutral temperatures, respectively.

The branching ratios for reaction (24) are taken to be $q[\bar{N}]/q[N] = 0.75/0.25$. Note that this reaction is not modelled self-consistently. Reaction (A22) implies that the direct photo-dissociation rate of NO is dependent on the amount of NO present. Since [NO] is unknown, we make the simplifying assumption of a constant rate of photo-dissociation of NO (while the atmosphere is sunlit), using values given by ROBLE and GARRY (1979).